Applied Catalysis A: General 382 (2010) 231–239

Contents lists available at ScienceDirect

Applied Catalysis A: General

journal homepage: www.elsevier.com/locate/apcata

Synthesis of nanozeolites and nanozeolite-based FCC catalysts, and their catalytic activity in gas oil cracking reaction

Gia-Thanh Vuong[a], Vinh-Thang Hoang[a], Dinh-Tuyen Nguyen[b], Trong-On Do[a,*]

[a] Department of Chemical Engineering, Laval University, 1065, avenue de La médecine, Québec G1V 0A6, Canada
[b] Institute of Chemistry, Vietnamese Academy of Science and Technology, Viet Nam

ARTICLE INFO

Article history:
Received 1 February 2010
Received in revised form 23 April 2010
Accepted 26 April 2010
Available online 24 May 2010

Keywords:
Nanozeolites
Formamide
Non-aqueous synthesis
FCC catalysts
FCC cracking

ABSTRACT

A new method for the synthesis of nanosized zeolites in organic solvents, such as formamide and toluene as crystallization medium instead of water, in the presence of organosilane has been developed. Organic solvents have a great impact on the synthesis of nanozeolites. Formamide, which has similar properties to water, is a good candidate as the solvent for the synthesis of nanosized zeolites. This synthetic method allows easy manipulation with the control of crystal sizes. In this study, different crystal sizes such as 25, 40 and 100 nm were prepared in toluene and formamide solvents. To study the effect of crystal nanosizes on the catalytic performance of nanosized zeolites, nanozeolite-based FCC catalysts were also prepared using different nanozeolite sizes as active component and silica as inactive matrix. The activity of these catalysts was evaluated with FCC feedstock. The results revealed a good correlation between the crystal size of zeolites and the activity: smaller nanozeolite-based FCC catalyst exhibits higher catalytic activity.

1. Introduction

Nanozeolites with the size of less than 200 nm have received much of interest recently, because of their great potential applications not only in catalysis and adsorption, but also in a variety of new applications including chemical sensing, medicine, optoelectronics etc. [1,2]. The decrease in the crystal sizes results in higher external surface areas, reduced diffusion path lengths, and more exposed active sites, which have an impact on the performance of the nanosized zeolites as compared to that of conventional zeolites of which the size is often of microns [1,3]. Besides the well known applications of such zeolites in catalysis and adsorption, nanozeolites can also find their applications as seeds and as building blocks for the preparation of mesoporous zeolitic materials [1,4–9]. Crystalline structure of zeolites with tridimensional network of well-defined micropores (pore diameter less than 15 Å) brings both (i) advantage and (ii) disadvantage. (i) This feature provides zeolite with a consistent adsorption behavior toward guest molecules. Only molecules of size less than or equal to pore size aperture can have access to the vast internal surface area of zeolites. Thus, when the catalytic reaction occurs inside the zeolite pores, zeolites can exhibit high selectivity toward small guest molecules [2,10,11]. (ii) However, the unique catalytic properties of zeolites are limited to reactant molecules having kinetic diameters below 15 Å, due to the pore size constraints. Reactions involving large molecules on zeolites hence must resort to only the external surface of zeolite [12].

The use of nanosized zeolites could overcome this limitation, the ratio of external to internal number of atoms increases rapidly as the particle size decreases, and zeolite nanoparticles have large external surface areas and high surface activity. The external surface acidity is of importance, when the zeolite is used as catalyst in reactions involving bulky molecule. The nanosized zeolites could bring better performance due to a high accessibility of active phase and high external surface area. For example, in catalytic cracking of gas oil, most of the hydrocarbon molecules are barred from zeolite pores and thus only the external surface of zeolite contributes to the gas oil conversion. Most of cracking of these molecules is realized on the interface of zeolite–matrix component of the FCC catalysts [13,14]. Rajagopalan et al. have shown that in cracking gas oil, when the crystallite size of zeolite decreases, both conversion and selectivity clearly increase [15]. On this aspect, the use of nanozeolites is a workaround and an improvement for FCC catalysts. Since the external surface of nanozeolites is expectedly higher and this type of surface is accessible, cracking of large hydrocarbon molecules on nanozeolites with high efficiency is possible. Hence a study of a nanozeolite-based FCC catalyst is of great interest.

Synthesis of nanozeolites has been studied extensively [1]. A common approach is to modify the general method of synthesis of zeolites, which is carried out in an aqueous phase [18–20]. Careful

* Corresponding author. Fax: +1 418 656 5993.
E-mail address: Trong-On.Do@gch.ulaval.ca (T.-O. Do).

0926-860X/$ – see front matter © 2010 Elsevier B.V. All rights reserved.
doi:10.1016/j.apcata.2010.04.049

adjustment of the parameters such as gel composition, temperature, crystallization time, aging time etc. can allow nanozeolites to form. The principle of the synthesis is derived from the classic nucleation and crystallization theory: facilitating the nucleation, which produces nuclei as much as possible; and controlling a subsequent slow growth of crystal particles. Ideally, the nucleation and growth processes should be completely separate from each other.

There are two possible mechanisms of nucleation in the synthesis of zeolites [21]: homogeneous nucleation and heterogeneous nucleation. Homogeneous nucleation occurs from the mother liquid while heterogeneous nucleation happens within the gel. Heterogeneous nucleation and growth are hardly separate process. Hence, regarding the synthesis of nanozeolites, it is very important to obtain the starting synthesis gel in the state of a "clear solution" or a clear gel solution in the hope that the homogeneous nucleation would take place instead of the heterogeneous one. Other factors such as aging, pH, crystallization time, gel composition are also subject to change to control the nucleation and growth process.

In this paper, we report a new route for the synthesis of nanozeolites of FAU by the soft controlling method using different types of solvents as crystallization medium instead of water. The crystal size of the nanozeolites can be manipulated to some extent by changing the solvent type. To evaluate the potential application, a series of FCC catalysts based on these nanozeolites with various particle sizes are also prepared. The obtained catalysts were tested against commercial catalysts in a standard test of gas oil cracking.

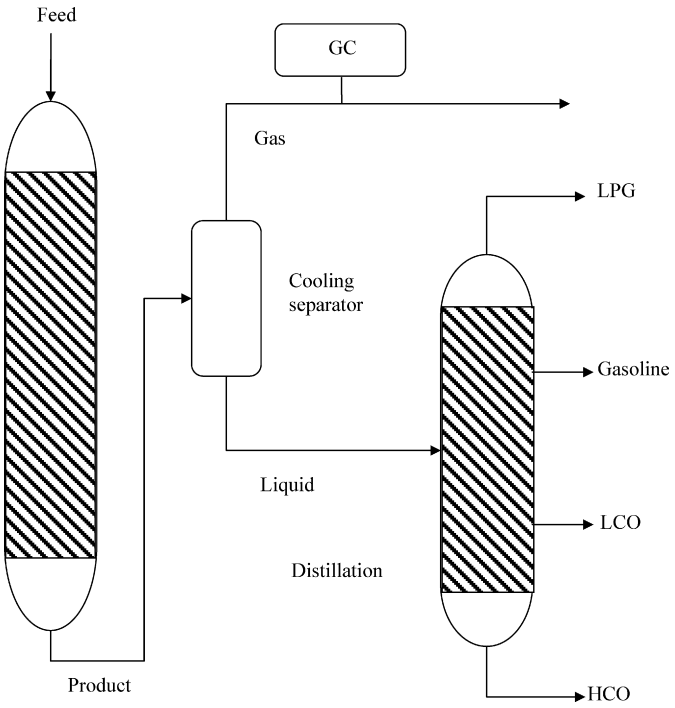

Scheme 1. Simplified diagram of the microactivity test MAT unit for cracking experiments.

2. Materials and methods

2.1. Synthesis of nanofaujasite

Three kinds of samples were prepared. The synthesis followed what we have reported [16]. In a typical procedure, Al(iPr)3 (19.5 g) was added into 78.36 g of TMAOH 25% under stirring for 3 h. Then 40.68 g of TEOS 98% was added. The stirring was continued overnight to make sure TEOS was completely hydrolyzed. Then, 64 mL of NaOH 0.1 M was added and stirred for another 3 h. The resulting clear solution was then aged at 90 °C for 2 (or 4) days to speed up the formation of protozeolitic species known as zeolite seeds. Subsequently, 10 g of the aged gel was added into 100 mL of hexadecyltrimethoxysilane (HDMT, 10%) containing toluene (or formamide). The clear homogeneous mixture was then transferred into an autoclave and heated for 5 days at 160 °C temperature. The silylated nanozeolite product was then recovered by centrifuge and washed with ethanol three times before drying at 100 °C for 24 h. The samples, prepared using toluene, were designated as FAU–TOL*x*D, while the ones using formamide were designated as FAU–FOR*x*D, where *x* is the aging time in day; the yield of synthesis was 41% and 47%, respectively. Zeolite Y reference was used from Strem Chemical.

2.2. Synthesis of nanofaujasite-based FCC catalysts

35 g of TEOS was dissolved in 100 mL of ethanol. To this mixture 10 g of as-made nanofaujasite was added. The mixture was stirred overnight and then evacuated under reduced pressure. The collected solid was dried at 100 °C for 24 h then calcinated at 600 °C for 6 h. The FCC catalyst samples were designated as FCC–FAU–TOL*x*D and FCC–FAU–FOR*x*D, where *x* is the aging time of zeolite gel in day.

2.3. Characterization

The FT-IR spectra were recorded using a Biorad FTS-60 spectrometer on sample wafers. Powder XRD patterns of the materials were recorded on a Philips X-ray diffractometer using nickel-filtered CuK_α ($\lambda = 1.5406$ Å) radiation.

The nitrogen adsorption/desorption measurements were carried out using an Omnisorp-100 automatic analyzer at −196 °C after degassing about 30 mg of calcined sample at 200 °C for at least 4 h under vacuum (10^{-4}–10^{-5} Torr). The specific surface area (S_{BET}) was determined from the linear part of the BET equation ($P/P_o = 0.05$–0.15). TEM images were obtained on a JEOL 200 CX transmission electron microscope operated at 120 kV. The samples for TEM were prepared by dispersing the fine powders of the products in slurry in ethanol onto honeycomb carbon copper grids. For scanning electron microscope (SEM), JEOL JSM-840 scanning electron microscope operated at 15 kV was used. Solid-state ^{29}Si MAS NMR spectra were recorded at room temperature on a Bruker ASX 300 spectrometer.

2.4. MAT cracking evaluation

Cracking experiments were performed in an automated fixed-bed microactivity test (MAT) unit (Zeton Automat IV), which was a modified version of ASTM D 5154. A simplified drawing of the MAT unit is shown in Scheme 1. The unit was equipped with collection systems for gas and liquid products. The distribution of gaseous products was analyzed by gas chromatographies. The boiling point (bp) range of the liquid products was determined by simulated distillation gas chromatography.

The catalysts were tested in the MAT unit at 510 °C with a weight hourly space velocity (WHSV) of 8 h^{-1}. All samples were steamed with 20% water vapor in N_2 at 550 °C for 24 h before the catalytic tests. MAT results reported include conversion, yields of dry gas (H_2, H_2S, C_1 and C_2), liquefied petroleum gas (LPG, i.e., C_3–C_4), gasoline (>C_5, bp up to 215 °C), LCO (bp 215–345 °C), heavy cycle oil (HCO, bp above 345 °C) and coke. Conversion was determined from the difference between the amount of feed and the amount of unconverted material defined as liquid product boiling above 215 °C (i.e., LCO + HCO). The same vacuum gas oil (VGO) was used to all MAT runs [17].

3. Results and discussion

3.1. Synthesis of nanozeolites

Crystallization of zeolites is complicated and sensitive to synthesis conditions. Its mechanism is still under debate. And a small change in the synthesis parameters could result in fruitless products. Hence it is very often that the products of the syntheses of nanozeolites using clear gel method are poorly crystalline and sometimes desired structures cannot be obtained [22,23].

An alternative approach is to apply a physical restriction into the synthesis environment [24–27]. The physical restriction provides a nanospace for the crystallization of zeolites inside it but prevents them from growing larger than the size of the nanospace. Porous carbon matrices, micro emulsion and methyl cellulose have been found being a good physical restrictor. Nevertheless, there are some difficulties that needed to be overcome: (i) the uniformity in the nanospace size of the restrictor of carbon matrix and methyl cellulose is not perfect, (ii) full introduction of synthesis gel into the restricting environment is almost impossible and (iii) the stability of the restrictor under the synthesis conditions are not acceptable.

Recently, we and other authors [16,28–30] have proposed a novel approach for the synthesis of nanozeolites. The idea is to apply a "soft" restriction on the crystal growth process. This is done using an organosilane to silanize the freshly formed nanozeolites during the crystallization, the resulting functionalized nanozeolites thus become stable toward the subsequent growth process. In our method, an organic solvent is introduced which can disperse these functionalized nanozeolites and completely protect them from the growth process. Hence, fine nanoparticles can be obtained. The introduction of organic solvent is an attractive option; the degree dispersion of the synthesis gel into the organic solvent depends largely on the affinity of the solvent toward water. A study of the influence of the solvent on the preparation of nanozeolites would be necessary and worthwhile. When a hydrophobic solvent is used, a large amount of the solvent is needed to obtain a complete dispersion of the synthesis gel. But for a hydrophilic solvent, the expectation is that gel dispersion would be easier. And thanks to the higher affinity toward the gel, higher impact on the crystal size of the final product is anticipated.

In our previous study, we used toluene as the solvent, which is hydrophobic [16,29,30]; hence it was difficult to obtain a homogeneous mixture of the aqueous synthesis gel in toluene. Thus, to adjust the affinity of this solvent to water, an addition of butanol as an additive was necessary. However, as the content of butanol increases the crystal size becomes larger; this is due to the fact that alcoholic systems tend to favor formation of large crystals [31]. So there is a compromise of butanol content; it should be sufficient for a complete dispersion of the synthesis gel but not too high so as the effect on crystal size is not significant. According to Qiu et al. [31], alcohol with dielectric constant lower than that of water would slow down the polymerization and thus the crystallization rate; hence large crystals are favored. So a good alternative solvent for the synthesis of functionalized nanozeolites should meet the following requirements: (i) high polarity and (ii) high solvating capacity. In short, the solvent must resemble water in terms of physicochemical properties as much as possible while maintaining dissolution capacity of organosilane agent.

Bearing that in mind it is clear that formamide would be a perfect solvent. The ability of formamide as a water replacement has been well established [32–34]. It should be noted that as formamide is an aprotic solvent, it contributes no protons to the synthesis gel. Hence, it is expected that the role formamide would be neutral during the synthesis process.

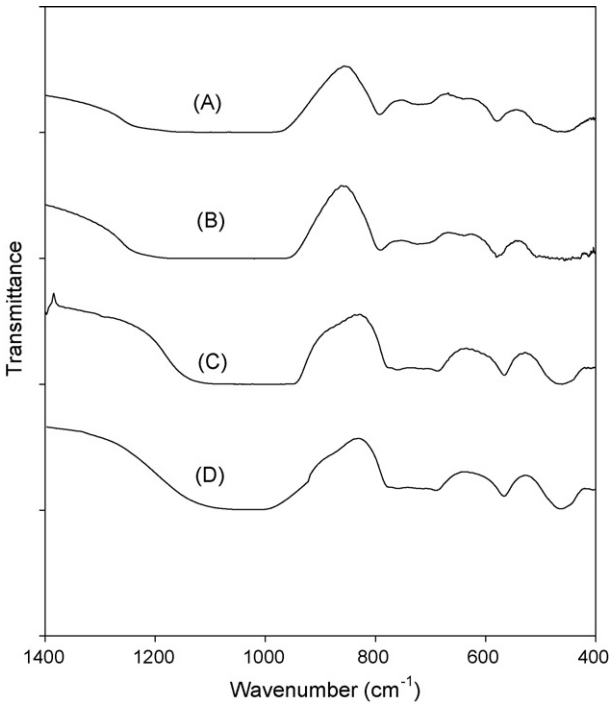

Fig. 1. FT-IR spectra of the prepared nanofaujasite samples: (A) FAU–TOL2D prepared using toluene and pre-heated zeolite gel for 2 days at 90 °C, (B) FAU–FOR2D prepared using formamide and pre-heated zeolite gel for 2 days at 90 °C, (C) FAU–FOR4D prepared using formamide and pre-heated zeolite gel for 4 days at 90 °C, and (D) zeolite Y reference.

To demonstrate the advantage of using formamide, we show here three representative samples of FAU nanozeolite, the first sample FAU–TOL prepared using toluene as the main solvent and the last two samples FAU–FOR prepared using formamide. The obtained FT-IR spectra in the region of framework vibrations are shown in Fig. 1. The band at 460 cm^{-1} is assigned to the internal vibration of TO_4 (T = Si or Al) tetrahedra. This vibration is always observable on aluminosilicate species [10]. The band at 565 cm^{-1} is attributed to the vibration of the double-ring D6R units [35]. This band can be regarded as a confirmation of the presence of a zeolitic structure. The bands at 685 and 775 cm^{-1} are assigned to external linkage symmetrical stretching and internal tetrahedral symmetrical stretching, respectively. Furthermore, the bands at 1010 and 1080 cm^{-1} are assigned to internal tetrahedral asymmetrical stretching and external linkage asymmetrical stretching, respectively [20]. Overall, the FT-IR spectra of these samples match well with the typical FT-IR absorption peaks of zeolite Y (Fig. 1).

The XRD patterns of the samples (Fig. 2) are identical to that of the FAU structure. There is a clear broadening of the reflections from the sample, which is attributed to small crystals. Furthermore, no evident peak at around $2\theta = 20–30°$ which is characteristic of amorphous phase, was observed indicating that the samples are highly crystalline.

Representative micrographs of the as-made nanofaujasite samples are shown in Fig. 3. The crystals appear very uniform. This is expected since the nanozeolite particles were protected from aggregation during the crystallization. The crystal size values of these samples FAU–TOL2D, FAU–FOR2D and FAU–FOR4D are 40, 25 and 100 nm, respectively. For the samples prepared in the presence of formamide, for example, the sample FAU–FOR4D which was prepared from the clear gel that was pre-heated for 4 days at 90 °C has larger crystal size than that of the sample FAU–FOR2D which was prepared from the gel pre-heated for 2 days at 90 °C. It is interesting to note that, while the FAU–FOR2D sample exhibits typical

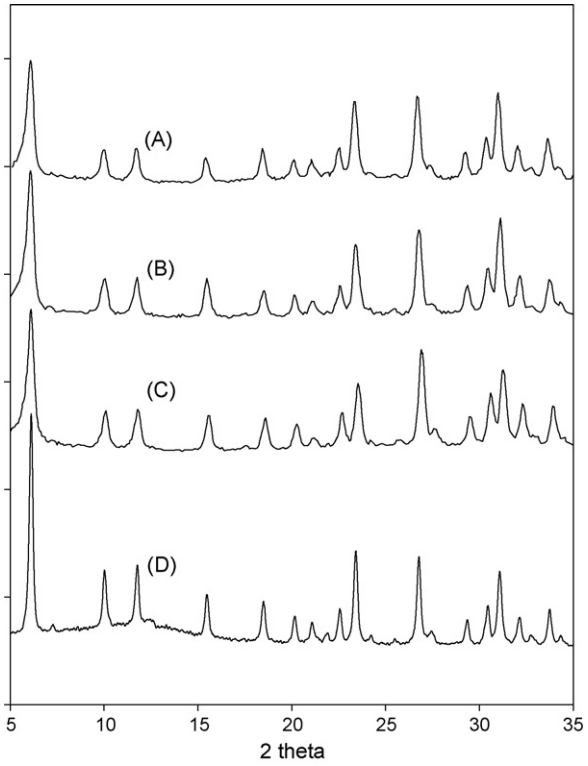

Fig. 2. XRD patterns of nanofaujasite samples prepared: (A) FAU–TOL2D in toluene, (B) FAU–FORM2D in formamide from the zeolite gel pre-heated at 90 °C for 2 days, (C) FAU–FORM4D in formamide from the zeolite gel pre-heated at 90 °C for 4 days, and (D) zeolite Y standard.

cubic single nanocrystals, the FAU–FOR4D sample shows spherical particles. The formation of these spherical particles is attributed to the Ostwald ripening effect, which aggregates the nanocrystals into larger one.

Fig. 4 shows the ^{29}Si MAS NMR spectra of the as-made faujasite prepared in aqueous medium in the absence of organosilane (conventional method) and silylated nanofaujasite samples prepared in solvent medium in the presence of organosilane. For the as-made silylated nanozeolite samples, besides the resonance peaks at −88, −95, −100 and −103 ppm corresponding to Si(3Al), Si(2Al), Si(1Al) and Si(0Al), respectively, the peak at −65 ppm attributed to R–C–Si–$(OSi)_3$ species. This peak results in the reaction between the silicon in the organosilane and the silanol groups of zeolite nuclei during the crystallization. The NMR broad peak at 50–70 ppm could be contributed to T2 and T3 which correspond to two and three OH groups consumed by one organosilane molecule. This peak at −65 ppm is absent in the faujasite sample prepared in aqueous medium in the absence of organosilane [36,37]. As seen in Fig. 4 for the silylated nanofaujasite samples, Q^4 signals became much broader with higher intensity as compared to those of the faujasite one. This means that the silanization led to the transformation of Q^3 to Q^4 silicon species during the crystallization. Thus, it can be concluded that the 3 samples of functionalized nanozeolites were obtained.

The pre-heating treatment of gel at 90 °C was an attempt to populate the protozeolitic species which were functionalized with organosilane agent for the next process of crystallization. The duration of the pre-heating process of zeolite gel is a significant parameter. It should be long to make sure that the population of protozeolitic species becomes sufficient. As the pre-heating treatment of zeolite gel was done, for the process of crystallization in the organic solvent, larger nanoparticles obviously grow at the expense

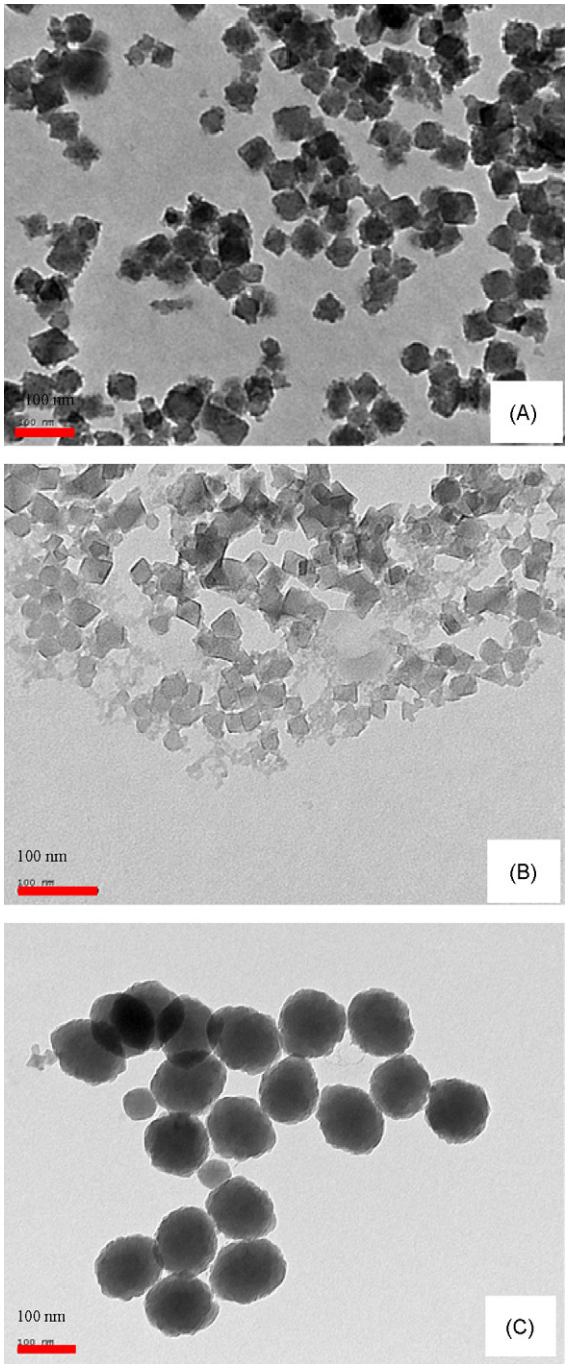

Fig. 3. TEM images of (A) the sample FAU–TOL2D prepared in toluene from the zeolite gel pre-heated at 90 °C for 2 days, (B) sample FAU–FOR2D prepared in formamide from the zeolite gel pre-heated at 90 °C for 2 days, and (C) the sample FAU–FOR4D prepared in formamide from the zeolite gel pre-heated at 90 °C for 2 days.

of smaller ones. As a result, these large species even functionalized with organosilane agent would be precipated. In this case, they settle down on the bottom of the teflon-line, and these species aggregate into larger ones.

However, the preparation using formamide allows production of nanozeolites with controlled crystal sizes. This fact is of important interest since it opens up a new method to synthesize nanozeolite crystals with predetermined crystal size. As discussed above, it is expected that protozeolitic species in synthesis gel pre-heated at 90 °C for 4 days would be larger in size than those in synthesis gel pre-heated for 2 days. Hence the dis-

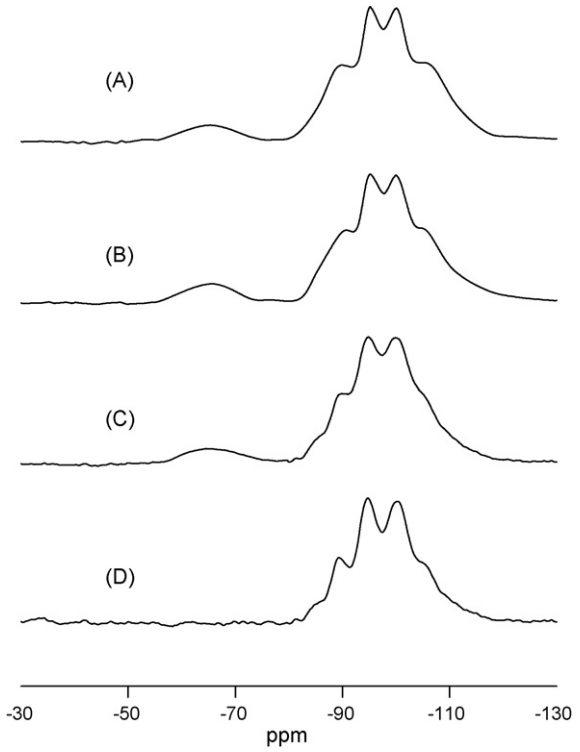

Fig. 4. ^{29}Si MAS NMR spectra of the as-made faujasite prepared in aqueous medium in absence of organosilane (conventional method) and silylated faujasite samples: (A) FAU–TOL4D using formamide pre-heated for 4 days, (B) FAU–FOR2D using formamide pre-heated for 2 days, (C) FAU–TOL2D using toluene pre-heated for 2 days, and (D) FAU-Standard using conventional method.

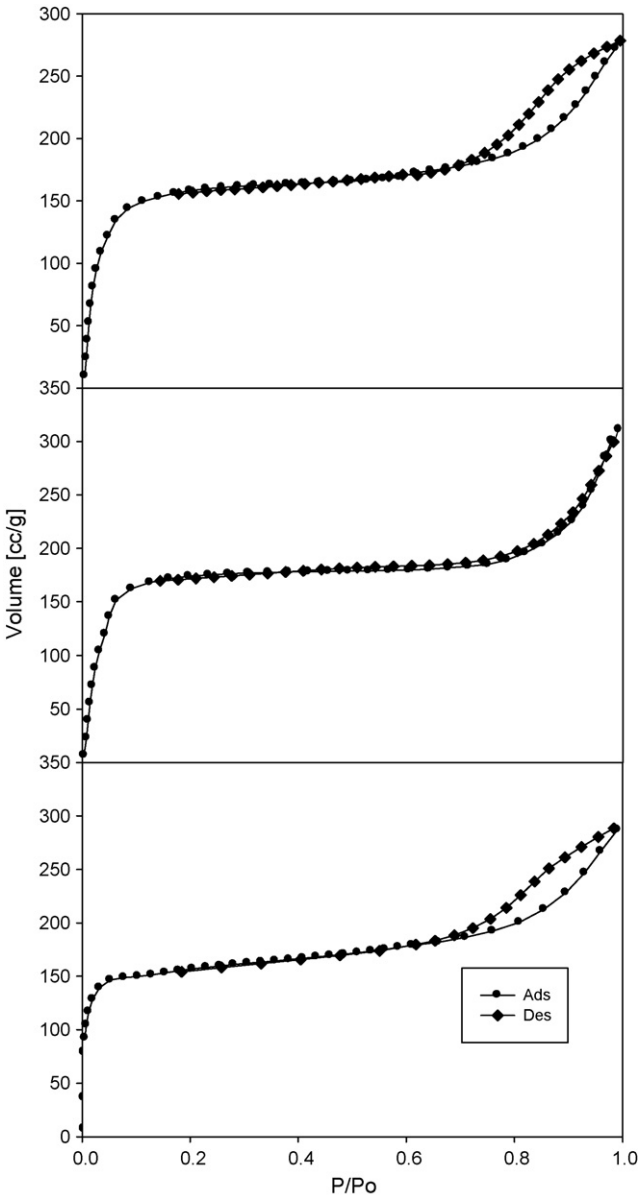

Fig. 5. N_2 adsorption desorption isotherms of (A) FAU–TOL2D prepared in toluene from the zeolite gel pre-heated at 90 °C for 2 days, (B) FAU–FOR2D prepared in formamide from the zeolite gel pre-heated at 90 °C for 2 days, and (C) FAU-FOR4D prepared in formamide from the zeolite gel pre-heated at 90 °C for 4 days.

persion of the gel pre-heated for 4 days in an organic solvent such as toluene would be more difficult since large protozeolitic species tend to aggregate at higher extent. Nevertheless, using formamide allows a tolerance toward these zeolite gels; hence it is well dispersed into the solvent. This is due to the fact that formamide has physicochemical properties similar to water, while still retaining great dissolution power toward the organosilane agents. However, the drawback could be the increase in crystal size. Fig. 5 shows the N_2 adsorption/desorption isotherms of different silylated nanofaujasite samples after calcination: FAU–TOL2D, FAU–FOR2D and FAU–FOR4D. The isotherms represent a steep rise in uptake at low relative P/P_o pressure and a flat curve following, which is typical for microporous materials. However, for FAU–TOL2D and FAU–FOR4D (Fig. 5A and C), an inflection at P/P_0 of 0.7–0.9 and a hysteresis loop are characteristics of capillary condensation and are related to the range of mesopores owing to the interparticles, while for FAU–FOR2D, a hysteresis loop was essentially not observed (Fig. 5B). This could be due to its smaller particle size (25 nm), as compared to the 40 and 100 nm size of the other ones. The specific surface areas are 505, 515 and 570 m^2/g, and the external surface areas based on *t*-plot calculation are 80, 115 and 65 m^2/g for FAU–TOL2D, FAU–FOR2D and FAU–FOR4D, respectively. In addition, the external surface areas of the samples are in agreement with the TEM analysis. The sample with a smaller size as indicated by TEM images shows higher external surface area. Some physicochemical properties of the faujasite samples are tabulated in Table 1.

3.2. Synthesis of FCC

XRD patterns of the nanozeolite-based FFC catalyst samples with different nanozeolite sizes are shown in Fig. 6. The presence of the FAU structure is observed; however, a broad peak at $2\theta = 20–30^\circ$ is available, implying the presence of amorphous matrix. The SEM images of these samples show that the FCC catalyst samples are

Table 1
Physicochemical properties of nanofaujasite samples.

Sample	Particle size (nm)	S_{BET} [m^2/g]	$S_{external}$[m^2/g]	Pore volume [cm^3/g]
FAU–TOL2D	40	505	80	0.43
FAU–FOR2D	25	520	130	0.60
FAU–FOR4D	100	570	65	0.45

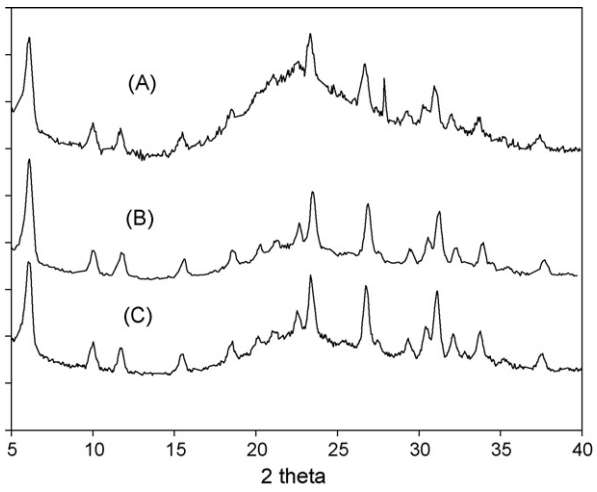

Fig. 6. XRD patterns of the nanozeolite-based FCC catalyst samples prepared from the corresponding 40, 24 and 100 nm nanozeolites: (A) FCC–TOL2D, (B) FCC–FOR2D and (C) FCC–FORM4D.

aggregated into micro-size particles, which are composed of uniform spheres of ~200 nm. These spheres are merely silica, and nanozeolites are well dispersed and incorporated along the silica spheres (Fig. 7). For these resulting FCC catalysts, the silica matrix could stabilize nanozeolites and increase the resistance of zeolite to steam deactivation and therefore increase the FCC catalyst real-life. The N_2 adsorption/desorption isotherms of these samples are shown in Fig. 8. The specific surface area values are 360, 355 and 315 m^2/g and the pore volumes are 0.90, 0.60 and 1.10 cm^3/g for FCC–FAU–TOL2D, FCC–FAU–FOR2D and FCC–FAU–FOR4D, respectively (Table 2) which are also namely FCC-40, FCC-25 and FCC-100.

3.3. Catalytic test

Before discussing the catalytic test results we should mention here two points: (i) nanozeolite particles are the main active components of these FCC catalysts and their activity in the cracking reaction is of our interest. The cracking of single hydrocarbon over nanozeolite has been reported by several authors [12,38,39]. This kind of reaction can provide a general suggestion on the potential of nanozeolite. However, it is necessary to evaluate the activity of nanozeolites in real-life application; hence the cracking of a typical feed for FCC cracking over nanozeolite-based catalysts was carried out and (ii) the matrix component of our nanozeolite-based catalysts was deliberately made almost neutral (amorphous silica) to the cracking reaction so that the impact of silica matrix as inactive matrix on the overall activity of the catalyst is negligent. Consequently, the activity of the catalysts can be supposed to stem from only the zeolite component. In a typical FCC catalyst, matrix component also plays an active role in the cracking of large hydrocarbon, contributing to the conversion as a whole [17]. Thus the activity of our nanozeolite-based catalysts regarding conversion is expected to be lower than that of the commercial ones.

The relation between conversion and catalyst-to-oil ratio is shown in Fig. 9. A general trend can be observed. The conversion increased with the catalyst-to-oil ratio and eventually it reached a plateau. This trend is explainable: as the catalyst-to-oil ratio rises the number of active sites available for the cracking reaction becomes higher resulting in higher conversion. As the ratio reaches a critical value, this effect is less pronounced; the conver-

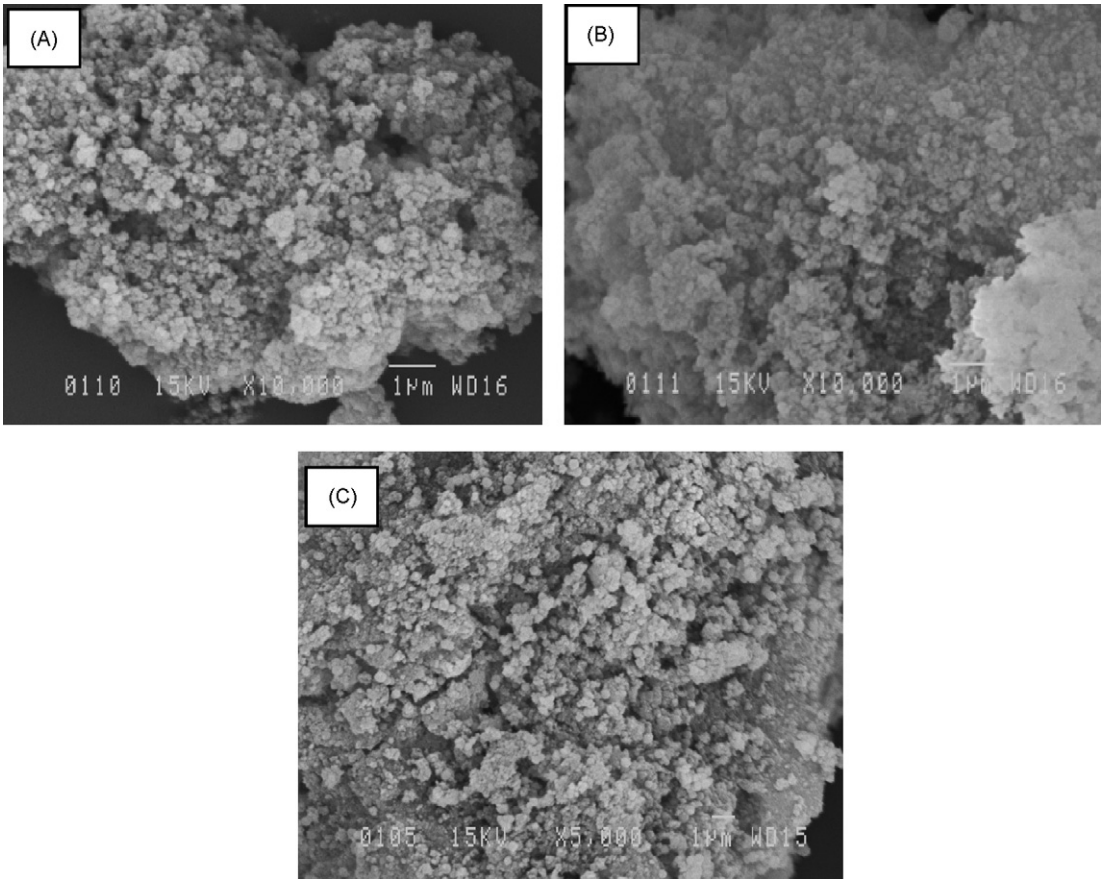

Fig. 7. SEM image of (A) FCC–FAU–TOL2D, (B) FCC–FAU–FOR2D and (C) FCC–FAU-FOR4D.

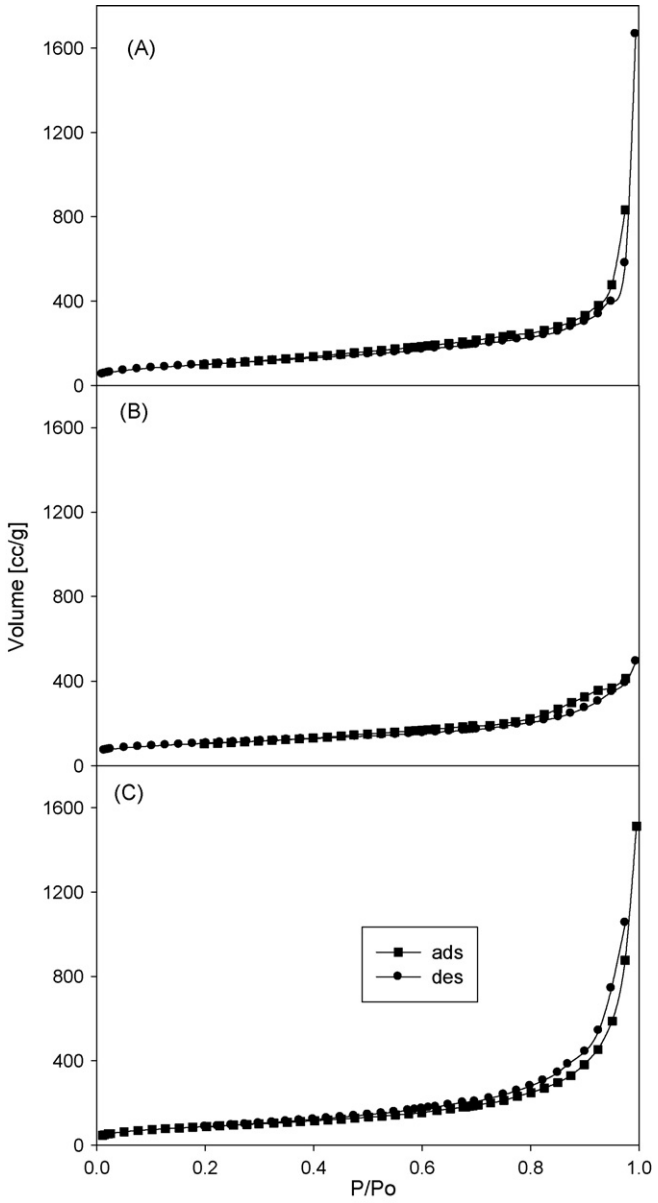

Fig. 8. N_2 adsorption desorption isotherms of (A) FCC–FAU–TOL2D, (B) FCC–FAU–FOR2D and (C) FCC–FAU–FOR4D.

Table 2
BET analysis of nanozeolite-based FFC catalyst samples.

Sample	S_{BET} [m^2/g]	$S_{external}$[m^2/g]	Pore volume [cm^3/g]
FCC–FAU–TOL2D	360	312	0.90
FCC–FAU–FOR2D	355	254	0.60
FCC–FAU–FOR4D	315	312	1.10

sion approaches a steady state. In agreement with our anticipation, the conversion over these catalysts is not very high. The highest value was observed on the sample FCC-25 (nanozeolite size ~25 nm), which is about 50%.

The most appealing conclusion drawn from the changed course of conversion is that it clearly demonstrates the ability of the impact of nanoparticles on catalytic activity. Reaction activity over the catalysts rises with the decrease in zeolite particle size. At the same catalyst-to-oil ratio the catalyst that bears the smallest nanoparticle size has the highest value among the three samples. Since the matrix components are identical and neutral among the catalysts, the change in activity is attributed to the larger external surface area, hence giving higher accessibility for large hydrocarbon molecules.

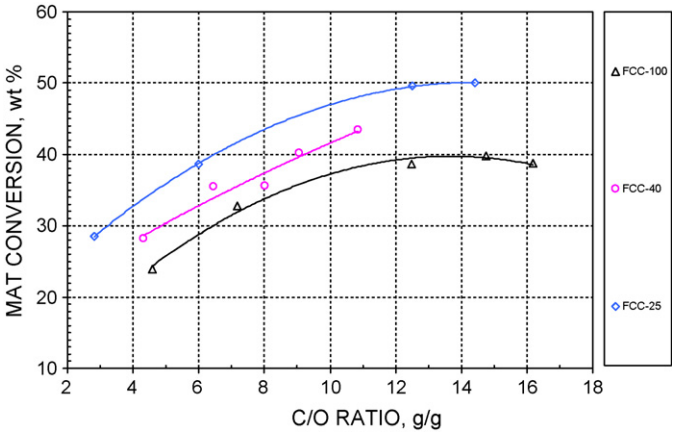

Fig. 9. Relationship between conversion and catalyst-to-oil ratio of different prepared FCC-samples.

The correlation of dry gas with conversion is plotted in Fig. 10. The dry gas is the lightest fraction of the cracking reaction. It contains C_1–C_2 hydrocarbons and other light gaseous molecules H_2, H_2S, CO and CO_2 etc. Dry gas is undesired since it has low value and hence its amount should be kept as low as possible. In most cases, dry gas is the product of thermal cracking and the overcracking of gasoline. Thus, it is reasonable that an increase in dry gas is observed at higher conversion. All the three catalyst samples exhibited a very low production of dry gas. As the conversion reaches the maximum value, the highest value of dry gas obtained over these catalysts is about only 2.5% wt. However, at the same given conversion, the yield of dry gas is in the following order: FCC-100 > FCC-40 > FCC-25. This order suggests that on nanozeolite, the secondary cracking and thermal cracking reactions are subdued.

LPG fraction is one of the products of cracking reaction that is valuable. The as-produced LPG contains C_3 and C_4 hydrocarbons which can be used in the commercial LPG and as a feedstock for further chemical upgrade to other chemicals of great value such as the octane boosters: MTBE and ETBE etc. As shown in Fig. 11, the LPG content increased with the rise of the conversion. Although the profiles of the yield curve of LPG over FCC-100 and FCC-40 are similar, in general, at a given conversion, the FCC-100 gave the highest LPG yield, followed by FCC-40 and FCC-25.

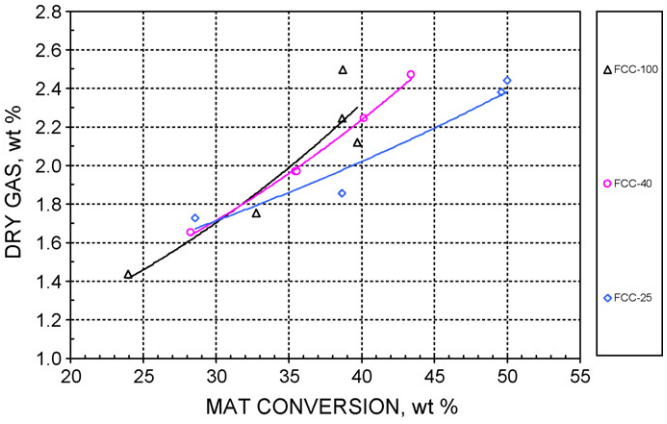

Fig. 10. Correlation of dry gas yield with conversion of different prepared FCC-samples.

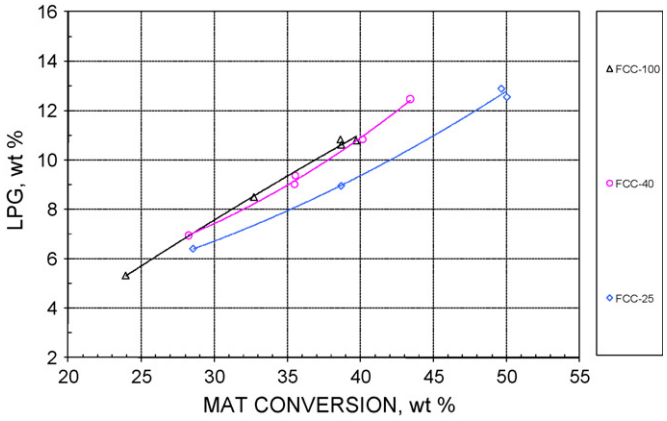

Fig. 11. Correlation of LCO yield with conversion of different prepared FCC-samples.

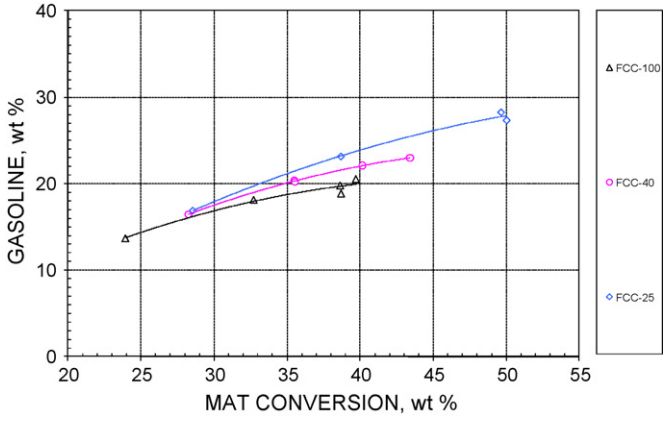

Fig. 12. Correlation between gasoline yield and conversion of different prepared FCC-samples.

Gasoline is the objective of the FCC process. The relation between conversion and gasoline yield is shown in Fig. 12. The relation profiles clearly demonstrate the advantage of nanozeolites. The catalyst containing smaller zeolite particles give higher gasoline yield, and the yield gap among these catalysts rises with the increase of conversion. Furthermore, an important parameter to evaluate the efficiency of an FCC catalyst is the gasoline selectivity, which is defined as the ratio of gasoline to conversion. The relationship between gasoline selectivity and conversion is shown in Fig. 13. Generally, the selectivity of gasoline decreased as the

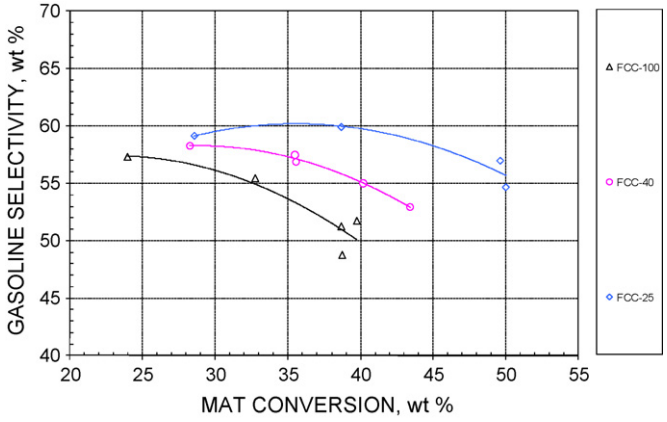

Fig. 13. Relationship between gasoline selectivity and conversion of different prepared FCC-samples.

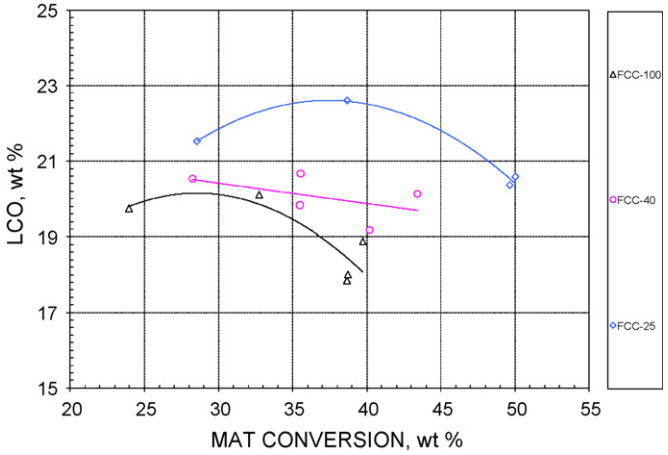

Fig. 14. Relationship between LCO yield and conversion.

conversion increased. However, the catalyst with smaller zeolite particles retained its higher selectivity.

LCO is the product of which the value changes seasonally. LCO is used as the feedstock to be upgraded to diesel and/or fuel oils. In an ideal cracking process, LCO is the intermediate product of a chain cracking reaction: HCO => LCO => gasoline.

LCO is both the product of the cracking of HCO and the reactant for the cracking to gasoline. The content of LCO produced can be taken as a parameter reflecting the competition between these two reactions. Cracking of large molecule cannot be done inside zeolite pores due to the small opening of its pores. In addition, the matrix component of the catalyst is essentially inactive. Hence, cracking of LCO and HCO must realize on the external surface of nanozeolites. Thus, the catalyst offering more of external surface area would give higher efficiency in cracking of large molecules. Taking into account the chain cracking scheme above, it is expected that, at the low conversion, the content of large molecules that are likely to be cracked is high; hence, the LCO produced rises as the conversion rises. However, with an increase of the conversion, the source of these molecules depleted; hence, after a maximum value of conversion, the rate of the cracking of large molecule is exceeded by the rate of cracking LCO; thus the content of LCO is decreased.

Fig. 14 shows the relationship between the LCO yield and the conversion. The convex curves of the LCO profiles over the FCC-100 and FCC-25 are noticed. For the FCC-40, the trend is different; the LCO yield exhibits a continuous decrease with the increase of conversion. But there is a consistent order among these three catalysts: at a given conversion, the yield of LCO is as follows: FCC-25 > FCC-40 > FCC-100.

HCO fraction is the undesired product of the FCC process. It contains the aromatic hydrocarbons that are difficult to crack and sulfur. Hence, HCO yield should be diminished to minimum. The relationships between HCO and conversion are in agreement with our expectation (Fig. 15): HCO yield is reduced using nanosized zeolites; the smaller the zeolite particles the lower the HCO yield.

Coke is an inevitable product and the only product that cannot be recovered. Being the catalyst poison and apparently giving no value in commercial applications, the coke formation is undesired and its amount should be as low as possible. The relationship between coke yield and conversion is shown in Fig. 16. The FCC-25 showed the least coke selectivity among the three catalysts.

In conclusion of the evaluation of FCC cracking, a clear trend has been noticed: the activity increases with the decrease in crystal size of the nanozeolites. This is due to the fact that cracking of FCC feed is heavily realized on external surface, which is higher on nanozeolite. The activity of the catalyst as a whole (the conversion)

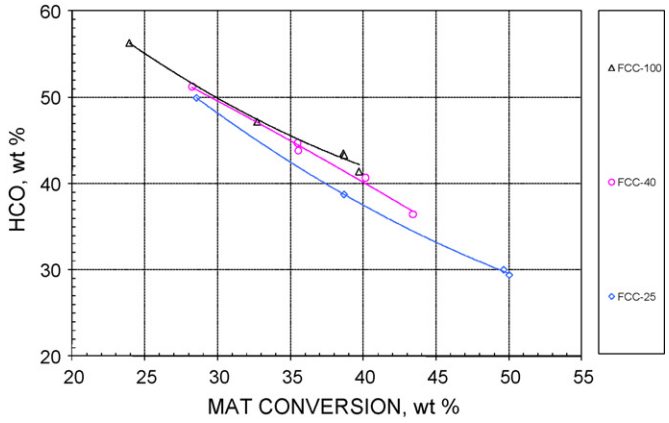

Fig. 15. Relation between HCO yield and conversion of different prepared FCC-samples.

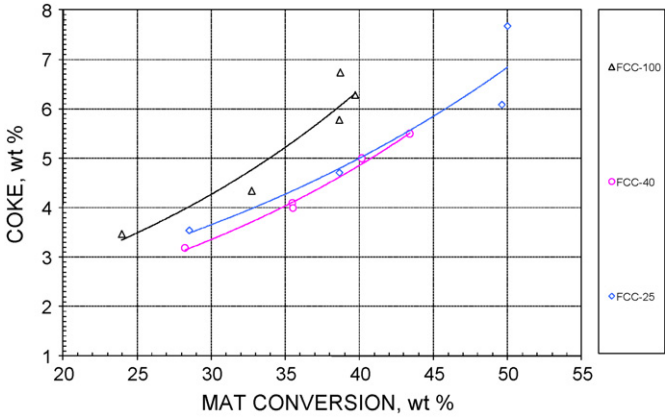

Fig. 16. Relationship between coke yield and conversion of different prepared FCC-samples.

was not very high; it is deliberate since the matrix component was made neutral, and it is likely that the acidity of nanozeolites is not sufficient. However, the addition of nanozeolite in FCC catalyst as main component or additive is an interesting option.

4. Conclusion

In this study, we have reported new methods of preparing nanozeolites using toluene and formamide solvents as crystallization medium instead of water. Different crystal sizes, e.g., 25, 40 and 100 nm, were prepared in toluene and formamide solvents. It was demonstrated that the solvents play an important role in giving the zeolite crystal with desired size. The key parameter that is important to choose the suitable solvent is its solvating power and its hydrophobicity. Nanozeolite-based FCC catalysts were prepared using silica as inactive matrix in order to study the effect of crystal size on the performance of nanozeolites. These FCC catalysts were evaluated with FCC feedstock. The relationship between gasoline selectivity and conversion is a function of nanozeolite size. In general, the performance of these catalyst is in the following order FCC-25 > FCC-40 > FCC-100.

Acknowledgments

This work was supported by the Natural Sciences and Engineering Research Council of Canada (NSERC) and the Research Application Development Society (SOVAR-Quebec). G.T.V. thanks the foundation of Laval University (FUL) for the scholarship. The authors thank Prof. S. Kaliaguine for stimulating discussions and comments.

References

[1] L. Tosheva, V.P. Valtchev, Chem. Mater. 17 (2005) 2494–2513.
[2] A. Corma, Chem. Rev. 97 (1997) 2373–2420.
[3] A. Corma, E. Sastre, J. Catal. 129 (1991) 177–185.
[4] T.-O. Do, A. Nossov, M.-A. Springuel-Huet, C. Schneider, J.L. Bretherton, C.A. Fyfe, S. Kaliaguine, J. Am. Chem. Soc. 126 (2004) 14324–14325.
[5] T.-O. Do, S. Kaliaguine, Angew. Chem. Int. Ed. 40 (2001) 3248–3251.
[6] T.-O. Do, S. Kaliaguine, Angew. Chem. Int. Ed. 41 (2002) 1036–1040.
[7] A. Karlsson, M. Stöcker, R. Schmidt, Micropor. Mesopor. Mater. 27 (1999) 181–192.
[8] L. Yu, Z. Wenzhong, J.P. Thomas, Angew. Chem. Int. Ed. 40 (2001) 1255–1258.
[9] Z. Zongtao, H. Yu, Z. Lei, W. Runwei, Y. Yi, Q. Shilun, Z. Dongyuan, X. Feng-Shou, Angew. Chem. Int. Ed. 40 (2001) 1258–1262.
[10] D. Breck, Zeolite Molecular Sieves: Structure, Chemistry, and Use, Wiley Interscience, New York, 1974.
[11] W.M.M.Ch. Baerlocher, D.H. Olson, Atlas of Zeolite Framework Types, Elsevier, 2001.
[12] B.W. Wojciechowski, A. Corma, Catalytic Cracking: Catalysts, Chemistry, and Kinetics, 1986.
[13] E.F.S. Aguiar, M.L.M. Valle, M.P. Silva, D.F. Silva, Zeolites 15 (1995) 620–623.
[14] M.A. Camblor, A. Corma, A. Martínez, F.A. Mocholí, J.P. Pariente, Appl. Catal. 55 (1989) 65–74.
[15] K. Rajagopalan, A.W. Peters, G.C. Edwards, Appl. Catal. 23 (1986) 69–80.
[16] G.-T. Vuong, T.-O. Do, Micropor. Mesopor. Mater. 120 (2009) 310–316.
[17] S. Al-Khattaf, Energy Fuels 17 (2003) 62.
[18] R. Ravishankar, C. Kirschhock, B.J. Schoeman, P. Vanoppen, P.J. Grobet, S. Storck, W.F. Maier, J.A. Martens, F.C. De Schryver, P.A. Jacobs, J. Phys. Chem. B 102 (1998) 2633–2639.
[19] P. Morales-Pacheco, F. Alvarez-Ramirez, P. Del Angel, L. Bucio, J.M. Dominguez, J. Phys. Chem. C 111 (2007) 2368–2378.
[20] P. Morales-Pacheco, F. Alvarez, L. Bucio, J.M. Domiì□nguez, J. Phys. Chem. C 113 (2009) 2247–2255.
[21] T.M. Davis, T.O. Drews, H. Ramanan, C. He, J. Dong, H. Schnablegger, M.A. Katsoulakis, E. Kokkoli, A.V. McCormick, R.L. Penn, M. Tsapatsis, Nat. Mater. 5 (2006) 400–408.
[22] C.S. Cundy, P.A. Cox, Chem. Rev. 103 (2003) 663–702.
[23] C.S. Cundy, J.O. Forrest, R.J. Plaisted, Micropor. Mesopor. Mater. 66 (2003) 143–156.
[24] C.J.H. Jacobsen, C. Madsen, T.V.W. Janssens, H.J. Jakobsen, J. Skibsted, Micropor. Mesopor. Mater. 39 (2000) 393–401.
[25] I. Schmidt, C. Madsen, C.J.H. Jacobsen, Inorg. Chem. 39 (2000) 2279–2283.
[26] H. Wang, B.A. Holmberg, Y. Yan, J. Am. Chem. Soc. 125 (2003) 9928–9929.
[27] Z. Chen, S. Li, Y.S. Yan, Chem. Mater. 17 (2005) 2262–2266.
[28] D.P. Serrano, J. Aguado, J.M. Escola, J.M. Rodriguez, A. Peral, Chem. Mater. 18 (2006) 2462–2464.
[29] G. T. Vuong, T.-O. Do, in: US (Ed.), US, 2008.
[30] G.T. Vuong, T.-O. Do, J. Am. Chem. Soc. 129 (2007) 3810–3811.
[31] S. Qiu, J. Yu, G. Zhu, O. Terasaki, Y. Nozue, W. Pang, R. Xu, Micropor. Mesopor. Mater. 21 (1998) 245–251.
[32] A. Lattes, E. Perez, I. Rico-Lattes, C. R. Chim. 12 (2009) 45–53.
[33] M. Almgren, S. Swarup, J.E. Loefroth, J. Phys. Chem. 89 (1985) 4621–4626.
[34] I. Rico, A. Lattes, J. Phys. Chem. 90 (1986) 5870–5872.
[35] G. Coudurier, C. Naccache, J.C. Vedrine, J. Chem. Soc., Chem. Commun. (1982) 1413–1415.
[36] B.Z. Zhan, M.A. White, M. Lumsden, Langmuir 19 (2003) 4205–4210.
[37] B.Z. Zhan, M.A. White, P. Fancy, C.A. Kennedy, M. Lumsden, Macromolecules 37 (2004) 2748–2753.
[38] P.B. Venuto, E.T. Habib Jr., Fluid Catalytic Cracking with Zeolite Catalysts, CRC Press, 1979.
[39] B.C. Gates, J.R. Katzer, G.C.A. Schuit, Chemistry of Catalytic Processes, McGraw-Hill College, 1979.